Novel Composites Polymer Electrolytes Based on Methylcellulose-pectin Blend Complexed With Potassium Phosphate and Ethylene Carbonate

Abdullahi Abbas Adam (ibneeabdullah234@gmail.com)
Universiti Teknologi PETRONAS
Hassan Soleimani
Universiti Teknologi PETRONAS
Muhammad Fadhlullah Bin Abd. Shukur
Universiti Teknologi PETRONAS
John Ojur Dennis
Universiti Teknologi PETRONAS
Yarima Mudassir Hassan
Universiti Teknologi PETRONAS
Bashir Abubakar Abdulkadir
Universiti Teknologi PETRONAS
Jemilat Yetunde Yusuf
Universiti Teknologi PETRONAS
Omar Sami Sultan Ahmed
Universiti Teknologi PETRONAS
Saba Ayub
Universiti Teknologi PETRONAS
Suleiman Shuaibu Abdullahi
Al-Qalam University Katsina

Research Article

Keywords: CPE, solution casting, EDLC, potential window

Posted Date: July 26th, 2022

DOI: https://doi.org/10.21203/rs.3.rs-1860435/v1

Abstract

In large-scale all-solid-state storage technologies, solid polymer electrolytes (SPEs) provide greater safety and longer cycle life than traditional liquid or gel polymer electrolytes. Polymer electrolytes (PEs) derived from biopolymers have been intensively explored for use in electrochemical devices due to their great flexibility, low cost, and environmental sustainability. However, biopolymer-based electrolytes cannot meet the expectations of practical applications at room temperature due to their low ionic conductivity. Over the years, improving the performance of this class of electrolytes has been the focus of intense research and development, notably polymer blending, plasticization, and structural functionalization. Here, we investigate the performance of an all-biopolymer solid electrolyte based on a methylcellulose-pectin blend doped with potassium phosphate. FESEM micrographs as well as the shifting and changing intensity of FTIR bands in the electrolyte specimens confirm the polyblend homogeneity with no phase separation. The increased amorphous fraction of the composites polymer electrolytes (CPEs) is seen in the XRD and DSC patterns of the plasticized and unplasticized samples. Impendence studies performed on the system recorded a maximum ionic conductivity of 1×10^{-5} Scm^{-1} by doping with 50 wt.% K_3PO_4. This value further increased to 5.9×10^{-5} Scm^{-1} upon adding 25 wt.% EC to the polymer system. This sample also possesses an electrochemical stability window of 4.24V and an ion transference number of 0.95.

1. Introduction

Human activities, particularly energy production and consumption, are the primary causes of severe environmental problems such as global warming and environmental degradation (A. A. Adam et al., 2020; Hassan et al., 2021). Researchers are now using biodegradable polymer membranes in energy systems such as metal-ion batteries, fuel cells, supercapacitors, and dye-sensitized solar cells to reduce the reliance on fossil fuels while boosting the use of alternative energy sources (M et al., 2020). In terms of energy storage, the electrochemical double-layer capacitors (EDLCs) which are a class of supercapacitors with superior properties are regarded as feasible alternatives to conventional batteries, thanks to their rapid charge-discharge rate, exceptional cycle stability, and high power density. The EDLC works on an electrostatic concept, in which electrolyte ions create dual layers on the interfacial surfaces of opposing electrodes. This technique underpins the general energy storage mechanism of every EDLC (Bashir Abubakar Abdulkadir et al., 2020; A. A. Adam et al., 2020; A. Asnawi et al., 2020; "Electrochemical supercapacitors for energy storage and delivery fundamentals and applications by Aiping Yu Victor Chabot Jiujun Zhang (z-lib.org).pdf,").

The polymer electrolytes (PEs) as an integral part of an EDLC have been intensively researched over the past 40 years due to their high ambient temperature conductivity, moldability, conformity, processability, and good electrode-electrolyte interaction (Abdullah, Ahmed, Tahir, Jamal, & Mohamad, 2021). Due to these exotic properties, current operations on flexible EDLCs and thin batteries with design freedom and high performance rely extensively on PEs. However, the ionic conductivity of these PEs needs to be improved to effectively meet commercial demand. Recently, PEs have been modified in a variety of ways to increase their ionic conductivity, electrochemical stability, and mechanical robustness. These modifications include the development of innovative polymers (Youcef et al., 2020), the cross-linking of two or more polymers (S. Tang et al., 2020), the mixing of polymers to produce polyblends (Mohamed, Shukur, Kadir, & Yusof, 2020), the introduction of plasticizers (M. H. Hamsan et al., 2020), and the addition of inorganic inert fillers/nanofillers (Črešnar et al., 2021) among others.

A typical PE is designed by the complexation of a host polymer(s) with an inorganic salt (e.g., potassium triphosphate). Conduction in SPEs occurs as a consequence of ion hopping within the host matrix and the polymer's segmental motion (Salleh, Aziz, Aspanut, & Kadir, 2016). Currently, SPE research is laying a greater emphasis on biopolymers as host materials, principally because biopolymers are ecologically friendly, non-toxic, and abundant in

nature. Additionally, they offer the potential to resolve some of the synthetic polymers' key shortcomings, among which include their insoluble nature in many organic solvents, non-biodegradability, and poor compatibility with certain inorganic salts (Jia et al., 2018; Monisha et al., 2017). Among natural-based polymers, methylcellulose (MC) is one of the most researched biopolymers due to its water solubility, the presence of hydroxyl groups in its chemical structure, and the existence of lone pairs of electrons at its oxygen atoms, which enables it to function as an electron donor since ionic conduction would occur in PEs only if the polymer matrix contains lone pairs of electrons. In addition to high mechanical strength, MC exhibits superior film-forming properties and a capacity to make transparent films (Omed Gh. Abdullah, Bakhtyar K. Aziz, Shujahadeen B. Aziz, & Mahdi H. Suhail, 2018a; M. H. Hamsan, Shukur, & Kadir, 2016; Kadir et al., 2017; Rudhziah, Rani, Ahmad, Mohamed, & Kaddami, 2015; Yusof, Woo, & Arof, 2016).

Similarly, pectin (PC), a common polysaccharide macromolecule ($C_6H_{10}O_7$) is extensively investigated recently. It is a carbohydrate biopolymer found mostly in citrus and apple products. Its molecular structure is composed of -1,4 linked galacturonic acid monomers that are partially methyl esterified. The anionic polymerization process was employed to extract pectin from its parent source (Naqash, Masoodi, Rather, Wani, & Gani, 2017; Perumal, Christopher Selvin, Selvasekarapandian, & Abhilash, 2019; Vahini & Muthuvinayagam, 2018). Due to its numerous OH groups, PC has a high number of coordination groups with salts, facilitating the development of complexation by ionic dissociation. As a consequence, PC can be blended with other polymers to produce a PE blend system with highly reduced crystallinity (Mohanapriya, Rambabu, Bhat, & Raj, 2020; Perumal, Christopher Selvin, Selvasekarapandian, & Sivaraj, 2019; Perumal, Selvasekarapandian, et al., 2019; Perumal & Selvin, 2021). In SPE technology Li and Na salts have been extensively utilized in the study of ionic conductivity of SPE systems. However, the ionic radius of K is greater than both Li and Na. Due to the high ionic radius of K salts, their lattice energy is lower than that of Li and Na salts. This makes the degree of salt salvation of K salts higher than that of Li and Na salts (Dey, Karan, Dey, & De, 2011). Notably, high-temperature resistant potassium salts dispersed in PVA/PVP polymer blend systems have been reported by Veena et al. (Veena & Lobo, 2018). The prepared PE recorded an ionic conductivity of 3.8×10^{-5} Scm^{-1} at ambient temperature.

In this study, we report a novel CPE consisting of MC and PC as host materials and potassium phosphate (K_3PO_4) and ethylene carbonate (EC) as the source of conducting ion and organic plasticizer, respectively. According to Abdulkadir et al. (B. A. Abdulkadir et al., 2021), the ionic conductivity of PE increases with the introduction of a plasticizer as a result of the plasticizer's ability to improve the flexibility of the polymer chain. Furthermore, Rajendran et al. (Rajendran & Saratha, 2021b) reported that EC possesses a superior dielectric constant, higher donor number, and elevated boiling temperature than other organic plasticizers. This study therefore uses a low molecular weight EC plasticizer at varying concentrations to increase the ionic conductivity of the prepared CPE at room temperature. This work will therefore demonstrate the suitability of MC/PC/K_3PO_4/EC CPE as a new type of simple, cheap, sustainable and highly stable CPE for electrochemical applications.

2. Materials And Methods

2.1 Materials

MC (viscosity of 4,000 cP) was purchased from Sigma Aldrich, Malaysia, PC (M_w of 30, 000 $gmol^{-1}$), K_3PO_4 (M_w of 212.27 $gmol^{-1}$) and glycerol (M_w of 92.09 $gmol^{-1}$) were purchased from R and M Chemicals, Malaysia. All chemicals were supplied by Evergreen Chemicals Supply (Selangor Malaysia) and used without further treatment. DI water was chosen as the only solvent throughout the experiment.

2.2 Methods

2.2.1 Synthesis of MC/PC polymer films

The methodology for the preparation of MC/PC based CPE is summarized in Fig. 1. In detail, appropriate masses of MC and PC (Table 1) were separately dissolved in 80ml DI water and stirred for several hours until fully dissolved. The samples were mixed and further stirred to obtain the MC/PC blend solution. This is followed by ultrasonication to ensure a homogenous mixture. Prepared samples were then cast on petri dishes and dried at 50 °C in anoven to obtain solid electrolyte films. Using a digital micrometer screw guage, an average film thickness of about 0.02–0.04cm was measured for the prepared films.

Table 1
Optimization of MC/PC blend ratio

wt % ratio of MC/PC	Mass of MC/PC (g)	Designation
0/100	0.0/1.0	AA01
10/90	0.1/0.9	AA02
20/80	0.2/0.8	AA03
30/70	0.3/0.7	AA04
40/60	0.4/0.6	AA05
50/50	0.5/0.5	AA06
60/40	0.6/0.4	AA07
70/30	0.7/0.3	AA08
80/20	0.8/0.2	AA09
90/10	0.9/0.1	AA10
100/0	1.0/0.0	AA11

2.2.2 Synthesis of K_3PO_4 doped MC/PC CPEs

Potassium-ion CPE was prepared by dispersing different concentrations of K_3PO_4 in a solution containing AA04. The concentration of K_3PO_4 was varied from 10 wt.% to 60 wt.% to examine the effect of K_3PO_4 on the ionic conductivity and electrochemical stability window of the prepared electrolytes. To ensure a homogenous mixture, the solution was stirred further for one hour after adding K_3PO_4 followed by 30 minutes of ultrasonication before casting and drying. For easy identification, the prepared samples were labelled AB01, AB02, AB03, AB04, AB05 and AB06.

2.2.3 Synthesis of EC plasticized MC/PC/K_3PO_4 CPEs

The preparation of plasticized samples is similar to that of MC/PC/K_3PO_4 with the only difference being that EC was added 10 min after adding K_3PO_4. Other procedures follow suit. Plasticized samples were labelled AC01, AC02, AC03, AC04, AC05 and AC06 for 5 wt.%, 10 wt.%, 15 wt.%, 20 wt.%, 25 wt.% and 30 wt.% EC respectively.

2.3 Characterization of electrolyte samples

Fourier transforms infrared (FTIR) analysis was used to examine the functional groups of the produced samples and their related band shifts. The FTIR analysis was performed in the 4000–400 cm^{-1} region with KBr pellets and a scanning resolution of 4 cm^{-1} using an FTIR spectrometer (Bruker Instruments, model Aquinox 55, Germany). The materials' structural properties were determined using a 40-kV Bruker D8 Advance X-ray diffractometer (XRD) operating at a current of 40 mA and a Ni-filtered Cu K graphite monochromator (Ś = 1.5406 Å). Field-Emission Scanning Electron Microscopy (FESEM) was used to analyse the surface morphology and percentage composition of component elements present in the samples. Differential scanning calorimetry (DSC) (Model DSC Q2000 V24.11, Oberkochen, Germany) was used to investigate the thermal behaviour of the PE. The glass transition temperature (T_g) of the samples was measured at a heating rate of 10 °Cm^{-1} from − 50 °C to 190 °C in a nitrogen (N_2) environment.

2.4 Electrochemical studies of solid electrolytes

Electrochemical studies were used to ascertain the ionic conductivity and operating potential window of each polymer electrolyte. The measurement was performed using the AUTOLAB/AUT51018 in a two-electrode setup. The CPE sample was sandwiched between two blocks of a stainless-steel sample holder with a 3.142 cm^2 surface area that was positioned opposite each other. Transference number measurement (TNM) was performed using a digital dc power supply (V&A Instrument DP3003).

3. Results And Discussion

3.1 Characterizations of CPEs

3.1.1 FTIR analysis

With the help of FTIR spectroscopy, it was possible to confirm the formation of a polymer blend between MC and PC. The band shifts for The FTIR spectral band assignments of prepared samples can be seen in Fig. 2 and Table 2, with the results showing that MC and PC have many functional groups in common. All wavenumbers found in all the samples were found to be consistent with previous literature (Omed Gh Abdullah, Bakhtyar K. Aziz, Shujahadeen B. Aziz, & Mahdi H. Suhail, 2018; Asnawi et al., 2021; Shujahadeen B Aziz et al., 2020; Kadir et al., 2017; Muthukrishnan et al., 2018; Nurhaziqah, Afiqah, Aziz, Aziz, & Hasiah, 2018; Perumal, Christopher Selvin, & Selvasekarapandian, 2018; Rajendran & Saratha, 2021b; Shuhaimi, Teo, Woo, Majid, & Arof, 2012; Vahini & Muthuvinayagam, 2018). Blending between MC and PC in the MC/PC polymer blend system can be confirmed by observing the polymers IR band shifts. The polymer blending could be correlated to IR spectral adjustments like band shifting or the development/disappearance of new spectral bands (Sohaimy & Isa, 2017).

Confirmation of MC backbone

1. According to the literature, the FTIR spectrum of pristine MC exhibit characteristic bands at the vicinity of 3250 and 2810 cm^{-1} belong to the O-H stretching, C-H asymetric stretching, respectively. Other spectral bands such as 1668, 1458 and 1058 cm^{-1} correspond to the COO^- asymmetric stretching, C-H rocking and C-O-C stretching MC, respectively (Abdullahi Abbas Adam et al., 2022; Asnawi et al., 2021; Shujahadeen B Aziz et al., 2020).
2. The O-H stretching of pure MC observed in this work lies between 3300 to 3650 cm^{-1} which is in close proximity to report by Asnawi et al. (Asnawi, Hamsan, Kadir, Aziz, & Yusof, 2020) and Aziz et al. (Shujahadeen B. Aziz et al., 2020).
3. The characteristic stretching peak found at ~2900 cm^{-1} belong to the prominent C-H scissoring of MC. In the work of Abdullah et al. (Omed Gh. Abdullah, Bakhtyar K. Aziz, Shujahadeen B. Aziz, & Mahdi H. Suhail, 2018b), this

band is found at 2910 cm^{-1} which is in close agreement with the finding in this work.

4. The ether band (characterized by COO^- asymmetric stretching) of pure MC is observed in this study between 1600 and 1750 cm^{-1}. Other absorption bands such as C-H rocking and C-O-C stretching of MC exist at 1300–1400 cm^{-1} and around 1100 cm^{-1} respectively. All these results are supported by previous literature (Aziz, Dannoun, Abdulwahid, et al., 2022; Faris et al., 2022; Vijaya, Selvasekarapandian, Sornalatha, Sujithra, & Monisha, 2017).
5. The tiny peaks seen around 946 cm^{-1} are the Infrared spectra characterization for MC (Nadirah, Ong, Saheed, Yusof, & Shukur, 2020).

Confirmation of PC backbone

1. For pristine PC film, literature has shown that the FTIR prominent bands are found within the proximity of 3334, 2910 and 1099 cm^{-1} which belong to O-H stretching, C-H stretching and C-O-C stretching of PC, respectively. The carboxylate ion bands of PC are found at 1652, 1422 cm^{-1} which represent the carbonyl (COO^-) asymmetric and symmetric stretching, respectively. In addition, typical PC is characteriszed by distictive bands around 1740, 1228 and 1010 cm^{-1} which are defined by the -$COOCH_3$ stretching of the ionized carboxymethyl group, the -CH-OH in the aliphatic cyclic secondary alcohol group and the -CH-O-CH- bending vibration of PC, respectively [22, 31, 37, 41].
2. In this study, the absorption bands seen at the vicinity of 3400 and 2880 cm^{-1} belong to the O-H stretching and C-H stretching of pure PC. These functional groups serve as coordination sites via hydrogen bonding. The band assignments for OH and CH stretches obtained in this study are in close agreement with some literature (Muthukrishnan et al., 2019; Perumal et al., 2018; Rajendran & Saratha, 2021a).
3. The C = O stretching vibration of the methyl-esterified carboxylic group (-$COOCH_3$) appears at 1620 cm^{-1}. This is an important functional group as it serve as complexation site with inorganic salt. A similar peak was reported by Vijaya et al. (Vijaya et al., 2017).
4. Based on literature, the positions of other less prominent functional groups of PC were seen around 1094 (Kiruthika, Malathi, Selvasekarapandian, Tamilarasan, & Maheshwari, 2020; Kiruthika et al., 2019) and 1371 cm^{-1} (Perumal et al., 2018) which belong to the C-C bond and the OH bending, respectively. However, the hydroxyl functional group of the OH bending vibration can equally serve as interaction site via hydrogen bonding due to the presence of oxygen atoms.

Confirmation of MC/PC polyblend

1. Upon mixing MC with PC, the synthesized polyblend film exhibit a shift in IR spectrum relative to conventional peaks of pristine MC and PC films (as shown in Table 1) due to the successful blending of MC with PC. The prominent O-H stretch is observed at 3370 cm^{-1} due to hydrogen bond interaction between the covalently bonded H atom of one polymer with the covalently bonded oxygen atom of the adjacent polymer. It can be seen that the hydrogen atom of hydroxyl band (O-H) in methylcellulose interact with glycosidic linkage (C-O-C) band in pectin (or vice versa) to form the MC/PC polymer blend. This leads to slight shift of the OH band of the blend systems to lower wavelength (relative to the OH band of pure PC). Similarly, the intensity of OH band in the blend systems down shifted, confirming the interaction of PC with MC via hydrogen bonding.
2. The CH stretching of MC/PC blend systems looks quite similar to that of pure PC, except for AA10 which contains a larger concentration of MC. This indicates that interaction between MC and PC barely occurs at the CH band of AA02 – AA09. Nevertheless, the alteration in the CH band of AA10 suggests a potential interaction in this functional group. This may be due to the larger concentration of electropositive hydrogen atoms linked to the carbon backbone of MC which might have interacted oxygen atoms of adjacent polymer.

3. The C = O stretch vary significantly for various combinations of MC and PC. This is evidently due to excellent interaction between hydrogen atom of one polymer with the carbonyl oxygen of the adjacent polymer. As the concentration of MC increases in the blend system, the C = O band becomes quite broader due to hydrogen bonding between MC and PC. Similarly, doublet bond CH bands are observed in the MC/PC blend, which become more prominent with increasing MC content. This band splitting is induced by the overtone of ring breathing mode vibrations and the presence of short-range ordering of the molecular orientation. This phenomenon is caused by the dipole-dipole interaction between two molecules and is related to the Fermi resonance of C = O stretching mode (Perumal, Christopher Selvin, Selvasekarapandian, Sivaraj, et al., 2019).
4. Other band assignments found in the MC/PC polyblend films formed due to the interaction of MC with PC are the IR band spectrum of C-H rocking (around 1350–1438 cm^{-1}) and the C-O-C stretching (1066 cm^{-1}). These bands do not show appreciable deviation from the pristine films which mean that interaction of MC with PC do not involve these functional groups appreciably. However, the oxygen atom in the C-O-C functional group can act as coordination site due to its high electronegativity.

Confirmation of complexation with K_3PO_4

1. When an MC/PC blend is doped with 10 to 50 wt. % K_3PO_4, the OH band of the polyblend becomes wider. As the salt concentration rises, the OH band equally downshifts, suggesting that complexation between the MC/PC blend (AA04) and K_3PO_4 has taken place. Apparently, the more K_3PO_4 added to AA04, the greater the concentration of K^+, and thus more electrons are pulled toward AA04 through the hydroxyl and carbonyl groups to form hydrogen bonds. The interaction of the conducting species (K^+) formed by K_3PO_4 increases the number of mobile ions, which increases the conductivity of the electrolytes. These FTIR data, therefore demonstrate that the oxygen atoms in those functional groups act as complexation sites for the salt's cation, resulting in the formation of dative bonds. Further increase in K_3PO_4 concentration causes the OH band (AB06) to upshift. This could be attributed to aglomeration of excess potassium ions which restricts ion migration.
2. The C-H band found at 2931cm^{-1} in the AA04 film expands as the concentration of K_3PO_4 increases upto 50 wt.%. This confirm that K_3PO_4 salt disrupts the MC/PC host polymer backbone. When the concentration of K_3PO_4 increases to 60 wt.%, the C-H peaks become more obvious with the protrusion of a sharp peak at around 2892 cm^{-1}, probably due to the aggregation of K^+.
3. Since complexation of MC/PC with K_3PO_4 is considered to occur majorly at the C = O peak owing to the existence of lone pair of electrons that attract free ions, raising the potassium salt concentration is found to cause a decrease in the transmittance intensity (and also a shift in the bandwidth of the doped samples to the lower wavelength zone) of the COO^- stretch. This apparent decrease in transmittance strength and shifting of bands indicate the development of complexes between salt cations and the carbonyl functional groups in the polymer blend matrix. This also demonstrates that the MC/PC host polymer and the added salt have significant interaction. A similar result was obtained by Nadirah et al. (Nadirah et al., 2020) showing a decrease in the intensity of MC/PAN blend with the addition of LiI salt.

Confirmation of EC plasticizer incorporation

EC is regarded an agent that might accelerate the dissociation of the ionic dopant K_3PO_4, leading to a greater dissociation of K^+ toward the MC/PC blend. In this system, it is claimed that EC develops a network with a shorter route, allowing K^+ to traverse and pass each site more freely. During the conduction process, weak bonds were established between K^+ and the oxygen atoms of EC before the K^+ jumped to the C = O of the CPE. Additionally, the

effective hop distance got shorter, causing the energy threshold to be reduced as well (Saadiah, Nagao, & Samsudin, 2021). Thus, it is anticipated that incorporation of EC will alter the IR spectra in the present CPE which signifies increase ionic conduction.

A careful examination of the FTIR spectra of the prepared CPEs reveals that the spectrum of each EC plasticizer incorporated AB05 film closely resembles that of unplqasticized AB05 film. However, the intensities of a few peaks vary significantly with increasing EC concentrations with only a slight shift in the positions of some of the peaks. The alterations in peak intensities strongly suggest that EC interact with the functional groups MC/PC/K_3PO_4 films.

1. In the IR spectrum of pure EC, a major doublet peak resulting from the C = O mode of EC is observed around 1700 cm^{-1}. The doublet peak is induced by the Fermi resonance of the C = O stretching mode, which is a result of dipole-dipole interaction between two EC molecules. The electropositively charged carbon atom of the carbonyl group in one EC molecule is electrostatically attracted to the electronegatively charged oxygen atom in another EC molecule (Nazir, Ismail, Zailani, Yahya, & Ali, 2021). Upon inclusion of EC into the MC/PC/K_3PO_4 system, slight modifications to the infrared intensity and locations were detected.
2. The vibration band at 2850 cm^{-1} in AB05 associated with the CH stretching mode has vanished as EC concentration was increased. The presence of EC has a significant impact on the amorphousness of the produced CPE. In addition, the interaction between salt and EC tends to minimize the coulombic interaction between the salt's cations and anions, resulting in an easier dissociation of salt in order to create a greater number of mobile charge carriers for high ionic transport (Perumal, Christopher Selvin, Selvasekarapandian, Sivaraj, et al., 2019). Moreover, the modification in the intensity and shift of the CH band vibrations suggests that the addition of EC might improve the diffusion of K^+ ions owing to the increase in free space and the enhanced polymer chain's segmental mobility. It is believed that the integration of K_3PO_4 and EC boosts the concentration of K^+ in CPE and ion–dipole complexations.
3. The COO^- symmetric stretching mode of AB05 in the polymer-salt system gives clear evidence of complexation through band shifting due to the presence of plasticizer. The polymer salt matrix also plays a significant role in polymer–ion and polymer–ion–plasticizer interactions in the CPEs due to the interaction of the plasticizer's surface acid group with the Lewis base upon the addition of EC. Potassium phosphate-anion and the surface groups of EC also exhibit the Lewis acid-base interaction within the polymer matrix. This mechanism decreases the Coulombic interaction between the salt's cation and anion, increasing the $K_2PO_4^-$ dissolvability thus more cations are available to coordinate with the oxygen atoms in the COO^- groups of the MC/PC blend. Further addition of EC results in a downshift in the COO^- transmittance intensity's band location for the stretching mode.
4. All of these changes in the FTIR spectrum apparently indicate that the salt and plasticizer had been effectively complexed and dissolved in the polymer blend.

Table 2
Functional groups of MC/PC and their corresponding band assignments

Functional groups Band Assignments	AA01	AA02	AA03	AA04	AA05	AA06	AA07	AA08	AA09	AA10	AA11
O-H stretching	3400	3454	3458	3470	3474	3502	3510	3523	3531	3543	3650
C-H asymmetric stretching	2880	2882	2885	2885	2885	2885	2885	2885	2889	2895	2900
COO^- asymmetric stretching	1620	1637	1649	1655	1659	1661	1665	1671	1675	1670	1750
C-H rocking in CH_2	1422	1425	1425	1425	1425	1425	1425	1425	1425	1433	1400
O-H bending	1371	1224	1220	1216	1212	-	-	-	-	-	-
C-O-C stretching	1094	1004	1006	1006	1008	1014	1018	1026	1030	1038	1100
*	-	957	954	949	947	988	929	933	937	941	946

Ref. AA01 (Muthukrishnan et al., 2018; Perumal et al., 2018; Rajendran & Saratha, 2021b; Vahini & Muthuvinayagam, 2018), AA02 – AA10 (Kadir et al., 2017; Muthukrishnan et al., 2018; Perumal et al., 2018; Rajendran & Saratha, 2021b; Shuhaimi et al., 2012) and AA11 (Omed Gh Abdullah et al., 2018; Asnawi et al., 2021; Shujahadeen B Aziz et al., 2020; Kadir et al., 2017; Nurhaziqah et al., 2018; Shuhaimi et al., 2012) * Infrared spectra characterization for MC (Nadirah et al., 2020)

3.1.2 XRD analysis

Figure 3a and 3b illustrates the XRD patterns produced from various ratios of MC/PC blended samples. Typically, MC is well-known for its broad semi-crystalline hump between 2=19–21°, which was caused by tightly bonded intermolecular hydrogen atoms spanning the short distances between its polymer chains. Additionally, hydrogen bonding happens when a hydrogen atom with deficient electron bonds with a highly electronegative atom (e.g. -O or -N). From the literature, pure MC also displays a substantial peak at 2=7–8° (Long et al., 2019; Nadirah et al., 2020; Nurhaziqah et al., 2018) while pure PC was found to have two large amorphous peaks located at about 7° and 20° (Kiruthika et al., 2019; Mendes, Esperança, Medeiros, Pawlicka, & Silva, 2017; Perumal, Christopher Selvin, Selvasekarapandian, & Sivaraj, 2019). In this work, it was discovered that pristine MC has crystalline peaks at 2=7.6° and 2=20.1°, whilst pristine PC contains wide bands at 2=7.4° and 2=20.5° (as shown in Fig. 3a). As the MC and PC were blended, their crystalline peaks progressively reduced, resulting in a more amorphous film, as seen in Fig. 3a. This is a clear indicator that MC and PC have effectively blended, as demonstrated by the FTIR investigations in the preceding section. AA04 was found to be the most amorphous of sample. Based on EIS investigations (to be described in detail in a later session), this sample has the greatest ionic conductivity.

The behaviour of the PE upon complexation with K_3PO_4 and EC is shown in Fig. 3b. As seen, the amorphous phase of the polymer matrix has increased with increased salt content. Pandi et al. (Pandi et al., 2016) reported that

incorporation of inorganic salt into PE increases the amorphousity of PE, thereby resulting in a decline in the energy barrier owing to the PE's segmental motion. Among the prepared polymer blend systems, AB04 observed to be the most amorphous sample. The reappearance of crystalline peak at 2=7.9° for AB06 could be due to the agglomeration of excess salt within the polymer matrix. Upon incorporation of EC into the polymer-salt complex, a further decrease in crystallinity was observed due to plasticization effect of EC. The amorphous region continues to improve with a further increase in EC content until an optimum is attained at 25 wt.% of EC, after which its crystallinity begins to reappear. Tiny peaks observed at 2Θ=24.6° and 2Θ=30.5° could be attributed to EC beginning to replace MC/PC host material in the SBE system. This observation is consistent with impedance studies which will be discussed further in another section.

3.1.3 FESEM micrograph

FESEM pictures may be used to test the compatibility of blend PEs and the interfaces within PEs. Additionally, surface exploration may provide information into how the structure and electrical properties of a material change as a consequence of different activities (Shujahadeen B Aziz et al., 2020). Earlier studies have shown that morphology analysis of polymers convey an overwhelming amount of information about surface changes (M. Hamsan, Aziz, Shukur, & Kadir, 2019; Kumar et al., 2014). In terms of crystallinity, the polymer family is divided into two distinct classes: crystalline polymers and amorphous polymers, which are defined by their degree of crystallinity. As shown in Fig. 4, the smooth FESEM surface morphology achieved for the blend system conveys information about the system's miscibility since the blending of MC with PC has increased the degree of amorphousness. Furthermore, the cross-sections of the films (insets) show no phase separations in all the blend films, implying that MC and PC are mutually miscible with one another and have been homogeneously blended. This result agrees well with the XRD pattern observed in the previous section.

Energy-dispersive X-ray spectroscopy (EDX) was employed to further verify the blending of MC with PC, as well as the elemental composition study of each sample. On the basis of their identified band spectra (shown in Fig. 5), it was established that C and O were the principal components of all samples. Similarly, the weight percentages, as well as the atomic percentages of the constituent elements found in each sample are presented in Table 3. As can be seen, oxygen atoms dominate over carbon atoms in all the samples except for AA11. This could be attributed to the presence of PC, which possesses numerous OH groups in the polyblend. The wt.% of oxygen atoms decreases as the concentration of PC reduces in the polyblend which confirms that PC contributes to the higher wt.% of oxygen atoms. Na spectra were identified in samples containing substantial amounts of PC (AA01 – AA09). On numerous occasions, sodium hydroxide (NaOH) was used as a pH stabiliser during the extraction and processing of PC (Hu, Ye, Chantapakul, Chen, & Zheng, 2020; Wandee, Uttapap, & Mischnick, 2019; Wang et al., 2020; Yang, Mu, & Ma, 2018; X. Yang et al., 2018). As a consequence, the existence of Na spectra may be ascribed to residual NaOH from the PC extraction procedure. However, as the concentration of PC in the polyblend system declines, the weight percentage of Na in the system decreases until it is completely absent (AA10 and AA11).

Table 3
Elemental composition of MC/PC films

Samples	Elements					
	C		O		Na	
	Weight %	Atomic %	Weight %	Atomic %	Weight %	Atomic %
AA01	42.39	49.65	56.45	49.64	1.16	0.71
AA02	45.45	52.71	53.78	46.82	0.77	0.47
AA03	46.94	54.20	52.33	45.36	0.73	0.44
AA04	47.44	54.68	51.94	44.95	0.62	0.37
AA05	47.46	54.69	51.96	44.96	0.58	0.35
AA06	47.58	54.80	51.92	44.89	0.51	0.31
AA07	47.79	55.02	51.69	44.67	0.51	0.31
AA08	49.10	56.30	50.46	43.44	0.44	0.26
AA09	48.27	55.47	51.31	55.47	0.42	0.25
AA10	49.94	57.06	50.06	42.94	-	-
AA11	51.82	58.90	48.18	41.10	-	-

3.1.4 DSC analysis

The thermal behaviour of the AA04, AB05, and AC05 complexes was studied using DSC analysis and the DSc thermograms are shown in Fig. 6. As shown, all samples display a wide endotherm phase transition between 40 and 130°C, which suggests the T_g of each CPE. To start with AA04, a single T_g seen on the DSC thermogram demonstrates that the MC and PC blend components are compatible. According to Shamsuri et al. (Shamsuri, Zaine, Yusof, Yahya, & Shukur, 2020), a single step transition of endothermic reaction observed in the DSC thermogram of MC/PVA film confirms the miscibility of the two polymers. Also, the effect of K_3PO_4 doping in MC/PC blend polymer on the T_g of prepared CPEs is equally investigated. The T_g value of AA04 (99.89°C) drops to 73.85°C when 50 wt.% K_3PO_4 is introduced to the MC/PC system. The decreased T_g value due to salt incorporation affirms that the polymer-salt's segment became less stiff in the amorphous phase structure, which has been previously confirmed by XRD analysis. As a result, the polymer host's T_g decreases, which is likewise linked to the PEs' increased ionic conductivity. To put it another way, when an electric field is applied to the AB04 system, the polymer chain network becomes more open to ions, which results in an increase in conductivity, since ions may flow freely across the polymer chain network.

At 25 wt.% EC content, the T_g decreases further to 67.59 ° C. This may be owing to the plasticization effect of the electrolyte caused by the presence of EC, which decreases the dipole–dipole interactions between polymer chains, hence softening the polymer morphology. Consequently, the drop in T_g implies an increase in the flexibility of the polymer chains, which facilitates the easy movement of ions across the polymer network by reducing the crystallinity of the polymer.

3.2 Electrochemical test

3.2.1 Conductivity studies

Batteries and supercapacitors used in high-power applications demand rapid charge/discharge rates; hence, electrolytes with high ionic conductivity are required for the proper operation of such devices (W. Tang et al., 2018). In this study, conductivity measurements were performed on CPEs using an impedance spectroscopy setup comprised of stainless steel (SS)/CPE/SS. The impedance plots for unplasticized and EC plasticized MC/PC/K_3PO_4 complexes are illustrated in Fig. 7. The resistance of each film is equivalent to the total of the bulk resistance obtained at the x-axis semicircle. At ambient temperature and within a frequency limit of 10^5–10^{-2} Hz, the influence of K_3PO_4 and EC on the ionic conductivity (σ) of an MC/PC composite system is determined using Eq. 1 (B, Km, M, V.S, & S, 2017);.

$$\sigma = \frac{l}{RS}$$

1

Here, l (cm), R (Ω) and S (cm^2) stand for the thickness of the CPE, bulk resistance, and the area of contact between the electrodes and the electrolyte, respectively. Furthermore, impedance curve shown in supplementary material (S1) illustrates the conventional impedance plots used to calculate ionic conductivity for selected MC/PC blend systems. Based on the impedance values obtained (from figure S1), highest ionic conductivity of 2.9×10^{-9} Scm^{-1} was obtained for the AA04 blend system, whereas pure MC (AA01), pure PC (AA11) and an equal ratio of MC and PC (AA06) exhibited a conductivity of 4.1×10^{-11} Scm^{-1}, 6.3×10^{-10} Scm^{-1} and 1.5×10^{-10} Scm^{-1} respectively. The increased ionic conductivity is attributed to decreased crystallinity in the blend system (Vahini & Muthuvinayagam, 2018), as will be discussed later.

The complex EIS curves of selected CPEs (AB01, AB05, AB06, AC01, AC05 and AC06) for varying concentrations of K_3PO_4 and EC are presented in Fig. 7. Other samples are shown in figures S2 and S3 in the supplementary material. As can be seen, the EIS curves show the quintessential behaviour of a typical EDLC, which consist of a symbolic spike and semi-circle at low and high frequencies, respectively. The high-frequency semi-circle is caused by parallel arrangements of bulk capacitance and bulk resistance (formed by immobilised polymer chains and cation migration, respectively), while the low-frequency spike is caused by blocking electrodes (Pandi et al., 2016). As a result of the increase in the number density of mobile charge carriers when K_3PO_4 was introduced, the ionic conductivity was optimised to 1×10^{-5} Scm^{-1} (AB05). When the salt and the polymer hosts come into contact, the K^+ ion disperses within the polymer matrix, thereby improving the conductivity of the polymer hosts. Increasing the concentrations of K_3PO_4 beyond 50 wt.% (SB06) results in a decrease in conductivity. This is because excess K_3PO_4 in the CPE may cause anions and cations to cluster so closely together that they form salt aggregates, obstructing the movement of free ions and reducing the number of free mobile ions inside the polymer host.

Furthermore, samples AC01-AC05 (Fig. 7 and S3) demonstrate that the addition of 5–25% EC results in a considerable inclination of the impedance spike toward higher frequency regions owing to the CPEs system's rapid dipolar relaxation. To support this, Aziz et al (Shujahadeen B Aziz et al., 2021) argues that plasticizers often increase ionic conductivity by increasing the charge carrier number of salt ions, hence enhancing salt dispersion and ion mobility. However, when additional EC (> 25 wt. %) is incorporated, the ionic conductivity decreases. Due to the high concentration of EC in the complex system, ion aggregates-contact ions forms, causing the ion flow through the CPE to slow down. As a consequence, ion mobility decreases, lowering the ionic conductivity of the system.

The variation of room temperature ionic conductivity of AC05 as a function of EC concentration is presented in Fig. 8. As can be seen, the conductivity of the CPE increases when EC was added, until it reaches a maximum value of 5.9×10^{-4} Scm^{-1} at a concentration of 25% EC (AC05). Due to the presence of EC, additional routes for ions to move have evolved, contributing to the conductivity rise. Along with functioning as a plasticizer, EC tends to weaken the Coulombic attraction between K_3PO_4 cations and anions. As a consequence, extra salts dissociated to liberate free mobile ions, thereby boosting the solution's ion density (Saadiah et al., 2021). Nevertheless, the addition of more than 25% wt. EC (AC06) leads to a decrease in conductivity. When plasticizer molecules are excess in the polymer-salt complexes, they displace the host fragments and cause the salt molecules to crystallise, reducing the host polymer's conductivity (Kadir et al., 2017). Thus, observed decrease in conductivity at 30% wt. EC was due to the recrystallization of K_3PO_4 in the SBE system.

3.2.2 Electrochemical potential window analysis

The electrochemical stability window is well recognised as one of the most critical elements in the practical use of an CPE. The stability window can be defined as a domain of potential in which the Faraday induced current does not flow through the electrolyte (Asnawi et al., 2021), and it is restricted within its cathodic and anodic sections, where the reduction and oxidation of the PEs and the salt ions take place (Abdullahi Abbas Adam et al., 2022). A very stable electrolyte is necessary for supercapacitors because of their rapid charging and discharging process, and to prevent deterioration of the electrolyte when a potential greater than its decomposition limit is applied (Dannoun et al., 2020; Fan et al., 2018). In this work, we determined the potential window stability of the CPEs by subjecting them to LSV testing using AUTOLAB/AUT51018. The samples were subjected to a voltage sweep with a constant scan rate of $10mVs^{-1}$ and a potential range of -4V to 4V and the results are shown in Fig. 9. As seen, all plasticized samples were found to exhibit a wider potential window compared to the unplasticized sample. For the optimum sample, a potential window of 4.24V was recorded. This indicates that the CPE is highly suitable for application in electrochemical systems since the threshold potential window for electrochemical device is 1V (Abdullahi Abbas Adam et al., 2022).

3.2.3 Transference number measurement

Solid-state ionics is a discipline of physics concerned with the ionic transport characteristics of materials that have a sufficiently high ionic conductivity (Shujahadeen B. Aziz et al., 2021). The TNM studies, along with LSV analysis are important parameters that determine the suitability of PE for use in EDLCs. In every EDLC, electrons and ions are, in theory the two charge-carrying species. The objective of TNM is to determine the identity of the predominant charge carrier species in the PE (Abdulwahid et al., 2021). The polarization curve for the comparatively highly conducting electrolyte is shown in Fig. 10. The measurement is taken by keeping the potential at 0.2 V, at which point the initial current begins, followed by a steady state. As a result of the polarization effect, an initial current (I_i) of 2.49 A is measured at the onset. Initially, both ions and electrons contribute to the first high value of the current, hence the large I_i recorded is due to the involvement of both ions and electrons. Before the steady state, the current decays significantly until it approaches saturation (as seen in Fig. 10). The absence of ionic species is responsible for this significant decrease in current until a steady-state current (I_{ss}) of 0.12 A is attained. In this condition, the cell is polarised and a current flow as a consequence of just electrons flowing as carrier conductors. Ion movement in the sample is prevented via the stainless-steel electrodes.

The values of the electronic (t_{elec}) and ionic (t_{ion}) transference numbers may be calculated using Equations (2) and (3);

$$t_{ion} = \frac{I_i - I_{ss}}{I_i}$$

2

$$t_{el} = 1 - t_{ion}$$

3

According to Aziz et al. (Aziz, Dannoun, Brza, et al., 2022), the transference number of the ion (t_{ion}) is an appropriate indicator of when it is almost equal to 1, given that ions are considered to be the principal charge carriers in PE systems. The computed values of t_e and t_{ion} for the AC05 sample are 0.048 and 0.952, respectively. The high value of t_{ion} indicates that ions, rather than electrons contribute majorly to the transport of charges.

Conclusions

In conclusion, the solution casting technique was used to fabricate CPEs containing K_3PO_4 as a novel conducting species. Ethylene carbonate (EC) was efficiently incorporated as a plasticizer into the MC/PC/K_3PO_4 electrolyte system at varying amounts to improve the conductivity of the system. The electrolyte containing 25 wt.% of EC has acquired the maximum ionic conductivity at room temperature (5.9×10^{-4} Scm^{-1}). The sample with the highest ionic conductivity had ions dominance with a t_{ion} of 0.95 and a high stability window of 4.24 V. Using the band frequencies from FTIR spectra, the molecular connection between the MC and PC hosts of the electrolyte was validated. XRD and DSC patterns have shown a substantial improvement in the amorphous phase for both plasticized and unplasticized blend systems.

Declarations

Ethics approval and consent to participate

No use of animals in this study.

Consent for publication

All the authors agree to publish this manuscript.

Availability of data and materials

The data will be made available by the corresponding author upon request.

Competing interests

The authors declare that they have no known competing financial interests or personal relationships that could have appeared to influence the work reported in this paper.

Funding

This study was funded by YUTP research grant 015LC0-317 and Universiti Teknologi PETRONAS (UTP), Malaysia via the Graduate Research Assistantship (GRA) scheme.

Authors contributions

Abdullahi Abbas Adam: Conceptualization, Methodology, Writing-original draft, Software, Formal analysis, Data curation and Formal analysis, Hassan Soleimani: Conceptualization, Supervision, Writing-review and editing, Methodology and Resources, Muhammad Fadhlullah Bin Abd. Shukur: Supervision, Writing-review and editing, Methodology, Funding acquisition and Project administration. John Ojur Dennis: Writing-review and editing, Validation, Formal analysis and Supervision. Bashir Abubakar Abdulkadir: Data curation, Software and Methodology. Yarima Mudassir Hassan: Investigation and Methodology. Jemilat Yetunde Yusuf: Data curation and Formal analysis. Omar Sami Sultan Ahmed: Methodology and Software. Saba Ayub: Visualization. Suleiman Shuaibu Abdullahi: Software. All authors have read and agreed to the published version of the manuscript.

Acknowledgements

Researchers acknowledge the Centre of Innovative Nanoscience and Nanostructures (COINN), Centralized Analytical Laboratory (CAL) and Electrical characterization Laboratory for providing research facilities.

Authors' information

Not applicable

References

1. Abdulkadir BA, Dennis JO, Abd. Shukur MFB, Nasef MME, Usman F, Adam AA, Adamu UA (2021) Dielectric Study of Gel Polymer Electrolyte Based on PVA-K2CO3-SiO2. *IOP Conference Series: Materials Science and Engineering, 1092*(1), 012066. doi:10.1088/1757-899x/1092/1/012066
2. Abdulkadir BA, Ojur Dennis J, Al-Hadeethi Y, Shukur MFBA, Mkawi EM, Al-Harbi N, Abbas Adam A (2020) Optimization of the Electrochemical Performance of a Composite Polymer Electrolyte Based on PVA-K2CO3-SiO2 Composite. Polymers 13(1). doi:10.3390/polym13010092
3. Abdullah OG, Ahmed HT, Tahir DA, Jamal GM, Mohamad AH (2021) Influence of PEG plasticizer content on the proton-conducting PEO:MC-NH4I blend polymer electrolytes based films. Results in Physics 23. doi:10.1016/j.rinp.2021.104073
4. Abdullah OG, Aziz BK, Aziz SB, Suhail MH (2018a) Surfaces modification of methylcellulose: Cobalt nitrate polymer electrolyte by sulfurated hydrogen gas treatment. *135*(35),46676. doi:https://doi.org/10.1002/app.46676
5. Abdullah OG, Aziz BK, Aziz SB, Suhail MH (2018b) Surfaces modification of methylcellulose: Cobalt nitrate polymer electrolyte by sulfurated hydrogen gas treatment. J Appl Polym Sci 135(35):46676. doi:https://doi.org/10.1002/app.46676
6. Abdullah OG, Aziz BK, Aziz SB, Suhail MH (2018) Surfaces modification of methylcellulose: Cobalt nitrate polymer electrolyte by sulfurated hydrogen gas treatment. J Appl Polym Sci 135(35). doi:10.1002/app.46676
7. Abdulwahid RT, Aziz SB, Brza MA, Kadir MFZ, Karim WO, Hamsan HM, Dannoun EMA (2021) Electrochemical performance of polymer blend electrolytes based on chitosan: dextran: impedance, dielectric properties, and energy storage study. J Mater Sci: Mater Electron 32(11):14846–14862. doi:10.1007/s10854-021-06038-7
8. Adam AA, Ojur Dennis J, Al-Hadeethi Y, Mkawi EM, Abdulkadir A, Usman B, Sani F, M (2020) State of the Art and New Directions on Electrospun Lignin/Cellulose Nanofibers for Supercapacitor Application: A Systematic Literature Review. Polym (Basel) 12(12):2884. doi:10.3390/polym12122884
9. Adam AA, Soleimani H, Shukur MFBA, Dennis JO, Abdulkadir BA, Hassan YM, Shamsuri NAB (2022) A new approach to understanding the interaction effect of salt and plasticizer on solid polymer electrolytes using

statistical model and artificial intelligence algorithm. J Non-cryst Solids 587:121597. doi:https://doi.org/10.1016/j.jnoncrysol.2022.121597

10. Asnawi A, Aziz SB, Nofal MM, Yusof YM, Brevik I, Hamsan MH, Kadir MFZ (2020) Metal Complex as a Novel Approach to Enhance the Amorphous Phase and Improve the EDLC Performance of Plasticized Proton Conducting Chitosan-Based Polymer Electrolyte. Membr (Basel) 10(6). doi:10.3390/membranes10060132
11. Asnawi ASFM, Hamsan MH, Aziz SB, Kadir MFZ, Matmin J, Yusof YM (2021) Impregnation of [Emim]Br ionic liquid as plasticizer in biopolymer electrolytes for EDLC application. Electrochim Acta 375:137923. doi:https://doi.org/10.1016/j.electacta.2021.137923
12. Asnawi ASFM, Hamsan MH, Kadir MFZ, Aziz SB, Yusof YM (2020) Investigation on electrochemical characteristics of maltodextrin – methyl cellulose electrolytes. Mol Cryst Liq Cryst 708(1):63–91. doi:10.1080/15421406.2020.1810954
13. Aziz SB, Brza M, Mishra K, Hamsan M, Karim WO, Abdullah RM (2020).. . Technology. Fabrication of high performance energy storage EDLC device from proton conducting methylcellulose: Dextran polymer blend electrolytes. *9*(2), 1137–1150
14. Aziz SB, Brza MA, Hamsan MH, Kadir MFZ, Muzakir SK, Abdulwahid RT (2020) Effect of ohmic-drop on electrochemical performance of EDLC fabricated from PVA:dextran:NH4I based polymer blend electrolytes. J Mater Res Technol 9(3):3734–3745. doi:https://doi.org/10.1016/j.jmrt.2020.01.110
15. Aziz SB, Dannoun E, Hamsan MH, Ghareeb HO, Nofal MM, Karim WO, Kadir MF (2021) A Polymer Blend Electrolyte Based on CS with Enhanced Ion Transport and Electrochemical Properties for Electrical Double Layer Capacitor Applications. Z A J P 13(6):930
16. Aziz SB, Dannoun EMA, Abdulwahid RT, Kadir MFZ, Nofal MM, Al-Saeedi SI, Murad AR (2022) The Study of Ion Transport Parameters in MC-Based Electrolyte Membranes Using EIS and Their Applications for EDLC Devices. *Membranes, 12*(2), 139. Retrieved from https://www.mdpi.com/2077-0375/12/2/139
17. Aziz SB, Dannoun EMA, Brza MA, Sadiq NM, Nofal MM, Karim WO, Kadir MFZ (2022) An Investigation into the PVA:MC:NH4Cl-Based Proton-Conducting Polymer-Blend Electrolytes for Electrochemical Double Layer Capacitor (EDLC) Device Application: The FTIR, Circuit Design and Electrochemical Studies. *Molecules, 27*(3), 1011. Retrieved from https://www.mdpi.com/1420-3049/27/3/1011
18. Aziz SB, Nofal MM, Abdulwahid RT, Ghareeb O, Dannoun H, Abdullah EMAM, Kadir R (2021) M. F. Z. Plasticized Sodium-Ion Conducting PVA Based Polymer Electrolyte for Electrochemical Energy Storage—EEC Modeling, Transport Properties, and Charge-Discharge Characteristics. *Polymers, 13*(5), 803. Retrieved from https://www.mdpi.com/2073-4360/13/5/803
19. B J, Km A, S J (2017) Development of a novel type of solid polymer electrolyte for solid state lithium battery applications based on lithium enriched poly (ethylene oxide) (PEO)/poly (vinyl pyrrolidone) (PVP) blend polymer. Electrochim Acta 235:210–222. doi:https://doi.org/10.1016/j.electacta.2017.03.118
20. Črešnar KP, Zemljič LF, Papadopoulos L, Terzopoulou Z, Zamboulis A, Klonos PA, Pissis P (2021) Effects of Ag, ZnO and TiO2 nanoparticles at low contents on the crystallization, semicrystalline morphology, interfacial phenomena and segmental dynamics of PLA. Mater Today Commun 27. doi:10.1016/j.mtcomm.2021.102192
21. Dannoun EMA, Aziz SB, Brza MA, Asnawi MMN, Yusof A, Woo YM, H. J (2020) The Study of Plasticized Solid Polymer Blend Electrolytes Based on Natural Polymers and Their Application for Energy Storage EDLC Devices. Polym (Basel) 12(11). doi:10.3390/polym12112531
22. Dey A, Karan S, Dey A, De SK (2011) Structure, morphology and ionic conductivity of solid polymer electrolyte. Mater Res Bull 46(11):2009–2015. doi:10.1016/j.materresbull.2011.07.008

23. Electrochemical supercapacitors for energy storage and delivery fundamentals and applications by Aiping Yu Victor Chabot Jiujun Zhang (z-lib.org).pdf
24. Fan L, Wang M, Zhang Z, Qin G, Hu X, Chen Q (2018) Preparation and characterization of PVA alkaline solid polymer electrolyte with addition of bamboo charcoal. Materials 11(5):679
25. Faris BK, Hassan AA, Aziz SB, Brza MA, Abdullah AM, Abdalrahman AA,... Saleh DI(2022) Impedance, Electrical Equivalent Circuit (EEC) Modeling, Structural (FTIR and XRD), Dielectric, and Electric Modulus Study of MC-Based Ion-Conducting Solid Polymer Electrolytes. *Materials; 15*(1), 170. Retrieved from https://www.mdpi.com/1996-1944/15/1/170
26. Hamsan M, Aziz SB, Shukur M, Kadir MJI(2019) Protonic cell performance employing electrolytes based on plasticized methylcellulose-potato starch-NH 4 NO 3. *25*(2),559–572
27. Hamsan MH, Aziz SB, Azha MAS, Azli AA, Shukur MF, Yusof YM, Kadir MFZ (2020) Solid-state double layer capacitors and protonic cell fabricated with dextran from Leuconostoc mesenteroides based green polymer electrolyte. Mater Chem Phys 241. doi:10.1016/j.matchemphys.2019.122290
28. Hamsan MH, Shukur MF, Kadir MFZ (2016) The effect of NH4NO3 towards the conductivity enhancement and electrical behavior in methyl cellulose-starch blend based ionic conductors. Ionics 23(5):1137–1154. doi:10.1007/s11581-016-1918-4
29. Hassan YM, Guan BH, Zaid HM, Hamza MF, Adil M, Adam AA, Hastuti K (2021) Application of Magnetic and Dielectric Nanofluids for Electromagnetic-Assistance Enhanced Oil Recovery: A Review. Crystals 11(2). doi:10.3390/cryst11020106
30. Hu W, Ye X, Chantapakul T, Chen S, Zheng J (2020) Manosonication extraction of RG-I pectic polysaccharides from citrus waste: Optimization and kinetics analysis. Carbohydr Polym 235:115982. doi:https://doi.org/10.1016/j.carbpol.2020.115982
31. Jia W, Li Z, Wu Z, Wang L, Wu B, Wang Y, Li J (2018) Graphene oxide as a filler to improve the performance of PAN-LiClO4 flexible solid polymer electrolyte. Solid State Ionics 315:7–13. doi:10.1016/j.ssi.2017.11.026
32. Kadir MFZ, Salleh NS, Hamsan MH, Aspanut Z, Majid NA, Shukur MF (2017) Biopolymeric electrolyte based on glycerolized methyl cellulose with NH4Br as proton source and potential application in EDLC. Ionics 24(6):1651–1662. doi:10.1007/s11581-017-2330-4
33. Kiruthika S, Malathi M, Selvasekarapandian S, Tamilarasan K, Maheshwari T (2020) Conducting biopolymer electrolyte based on pectin with magnesium chloride salt for magnesium battery application. Polym Bull 77(12):6299–6317. doi:10.1007/s00289-019-03071-9
34. Kiruthika S, Malathi M, Selvasekarapandian S, Tamilarasan K, Moniha V, Manjuladevi R (2019) Eco-friendly biopolymer electrolyte, pectin with magnesium nitrate salt, for application in electrochemical devices. J Solid State Electrochem 23(7):2181–2193. doi:10.1007/s10008-019-04313-6
35. Kumar KK, Ravi M, Pavani Y, Bhavani S, Sharma A, Rao VN(2014) J. J. o. M. S. Investigations on PEO/PVP/NaBr complexed polymer blend electrolytes for electrochemical cell applications. *454*, 200–211
36. Long M-C, Xia L-T, Lyu T-B, Wang T, Huang T, Chen L, Wang Y-Z (2019) A green and facile way to prepare methylcellulose-based porous polymer electrolytes with high lithium-ion conductivity. Polymer 176:256–263. doi:10.1016/j.polymer.2019.05.056
37. M MN, Aziz SB, Hadi JM, Abdulwahid RT, Dannoun EMA, Marif AS, Kadir MFZ (2020) Synthesis of Porous Proton Ion Conducting Solid Polymer Blend Electrolytes Based on PVA: CS Polymers: Structural, Morphological and Electrochemical Properties. Mater (Basel) 13(21). doi:10.3390/ma13214890

38. Mendes JP, Esperança JMSS, Medeiros MJ, Pawlicka A, Silva MM (2017) Structural, morphological, ionic conductivity, and thermal properties of pectin-based polymer electrolytes. Mol Cryst Liq Cryst 643(1):266–273. doi:10.1080/15421406.2016.1263111
39. Mohamed A, Shukur M, Kadir M, Yusof YJ(2020) J. o. P. R. Ion conduction in chitosan-starch blend based polymer electrolyte with ammonium thiocyanate as charge provider. *27*, 1–14
40. Mohanapriya S, Rambabu G, Bhat SD, Raj V (2020) Pectin based nanocomposite membranes as green electrolytes for direct methanol fuel cells. Arab J Chem 13(1):2024–2040. doi:https://doi.org/10.1016/j.arabjc.2018.03.001
41. Monisha S, Mathavan T, Selvasekarapandian S, Milton Franklin Benial A, Aristatil G, Mani N, Vinoth pandi D (2017) Investigation of bio polymer electrolyte based on cellulose acetate-ammonium nitrate for potential use in electrochemical devices. Carbohydr Polym 157:38–47. doi:https://doi.org/10.1016/j.carbpol.2016.09.026
42. Muthukrishnan M, Shanthi C, Selvasekarapandian S, Manjuladevi R, Perumal P, Selvin C, P (2018) Synthesis and characterization of pectin-based biopolymer electrolyte for electrochemical applications. Ionics 25(1):203–214. doi:10.1007/s11581-018-2568-5
43. Muthukrishnan M, Shanthi C, Selvasekarapandian S, Manjuladevi R, Perumal P, Selvin C, P (2019) Synthesis and characterization of pectin-based biopolymer electrolyte for electrochemical applications. Ionics 25(1):203–214. doi:10.1007/s11581-018-2568-5
44. Nadirah BN, Ong CC, Saheed MSM, Yusof YM, Shukur MF (2020) Structural and conductivity studies of polyacrylonitrile/methylcellulose blend based electrolytes embedded with lithium iodide. Int J Hydrog Energy 45(38):19590–19600. doi:https://doi.org/10.1016/j.ijhydene.2020.05.016
45. Naqash F, Masoodi FA, Rather SA, Wani SM, Gani A (2017) Emerging concepts in the nutraceutical and functional properties of pectin—A Review. Carbohydr Polym 168:227–239. doi:https://doi.org/10.1016/j.carbpol.2017.03.058
46. Nazir K, Ismail SNS, Zailani NAM, Yahya MZA, Ali AMM(2021) Effect of ethylene carbonate (EC) plasticizer on epoxidized 30% poly(methyl methacrylate)-grafted natural based polymer electrolytes for lithium batteries. *AIP Conference Proceedings, 2332*(1), 100002. doi:10.1063/5.0043681
47. Nurhaziqah AMS, Afiqah IQ, Aziz MFHA, Aziz NAN, Hasiah S(2018) Optical, Structural and Electrical Studies of Biopolymer Electrolytes Based on Methylcellulose Doped with Ca(NO3)2. *IOP Conference Series: Materials Science and Engineering, 440*. doi:10.1088/1757-899x/440/1/012034
48. Pandi DV, Selvasekarapandian S, Bhuvaneswari R, Premalatha M, Monisha S, Arunkumar D, Junichi K (2016) Development and characterization of proton conducting polymer electrolyte based on PVA, amino acid glycine and NH4SCN. Solid State Ionics 298:15–22. doi:10.1016/j.ssi.2016.10.016
49. Perumal P, Selvin C, Selvasekarapandian S (2018) Characterization of biopolymer pectin with lithium chloride and its applications to electrochemical devices. Ionics 24(10):3259–3270. doi:10.1007/s11581-018-2507-5
50. Perumal P, Christopher Selvin P, Selvasekarapandian S, Abhilash KP (2019) Bio-host pectin complexed with dilithium borate based solid electrolytes for polymer batteries. Mater Res Express 6(11). doi:10.1088/2053-1591/ab4724
51. Perumal P, Christopher Selvin P, Selvasekarapandian S, Sivaraj P(2019) Structural and Electrical Properties of Bio-polymer Pectin with LiClO4 Solid Electrolytes for Lithium Ion Polymer Batteries. *Materials Today: Proceedings, 8*, 196–202. doi:10.1016/j.matpr.2019.02.100
52. Perumal P, Christopher Selvin P, Selvasekarapandian S, Sivaraj P, Abhilash KP, Moniha V, Devi M, R (2019) Plasticizer incorporated, novel eco-friendly bio-polymer based solid bio-membrane for electrochemical clean

energy applications. Polym Degrad Stab 159:43–53. doi:https://doi.org/10.1016/j.polymdegradstab.2018.11.013

53. Perumal P, Selvasekarapandian S, Abhilash KP, Sivaraj P, Hemalatha R, Selvin PC (2019) Impact of lithium chlorate salts on structural and electrical properties of natural polymer electrolytes for all solid state lithium polymer batteries. Vacuum 159:277–281. doi:https://doi.org/10.1016/j.vacuum.2018.10.043
54. Perumal P, Selvin PC (2021) Boosting the performance of electric double layer capacitor via engaging pectin macromolecular electrolyte with elevated ionic conductivity and potential window stability. Chem Eng J Adv 8:100178. doi:https://doi.org/10.1016/j.ceja.2021.100178
55. Rajendran S, Saratha R(2021a) An evaluation of solid-state electrolyte based on pectin and lithium bis (trifluoromethanesulphonyl)imide for lithium-ion batteries. *Materials Today: Proceedings, 47*, 819–824. doi:https://doi.org/10.1016/j.matpr.2020.12.557
56. Rajendran S, Saratha R(2021b) An evaluation of solid-state electrolyte based on pectin and lithium bis (trifluoromethanesulphonyl)imide for lithium-ion batteries. *Materials Today: Proceedings*. doi:10.1016/j.matpr.2020.12.557
57. Rudhziah S, Rani MSA, Ahmad A, Mohamed NS, Kaddami H (2015) Potential of blend of kappa-carrageenan and cellulose derivatives for green polymer electrolyte application. Ind Crops Prod 72:133–141. doi:10.1016/j.indcrop.2014.12.051
58. Saadiah MA, Nagao Y, Samsudin AS (2021) Enhancement on protonation (H+) with incorporation of flexible ethylene carbonate in CMC–PVA–30 wt % NH4NO3 film. Int J Hydrog Energy 46(33):17231–17245. doi:https://doi.org/10.1016/j.ijhydene.2021.02.187
59. Salleh NS, Aziz SB, Aspanut Z, Kadir MFZ (2016) Electrical impedance and conduction mechanism analysis of biopolymer electrolytes based on methyl cellulose doped with ammonium iodide. Ionics 22(11):2157–2167. doi:10.1007/s11581-016-1731-0
60. Shamsuri NA, Zaine SNA, Yusof YM, Yahya WZN, Shukur MF (2020) Effect of ammonium thiocyanate on ionic conductivity and thermal properties of polyvinyl alcohol–methylcellulose–based polymer electrolytes. Ionics 26(12):6083–6093. doi:10.1007/s11581-020-03753-9
61. Shuhaimi NEA, Teo LP, Woo HJ, Majid SR, Arof AK (2012) Electrical double-layer capacitors with plasticized polymer electrolyte based on methyl cellulose. Polym Bull 69(7):807–826. doi:10.1007/s00289-012-0763-5
62. Sohaimy M, Isa MJPB(2017) Ionic conductivity and conduction mechanism studies on cellulose based solid polymer electrolytes doped with ammonium carbonate. *74*(4),1371–1386
63. Tang S, Lan Q, Xu L, Liang J, Lou P, Liu C, Cheng S (2020) A novel cross-linked nanocomposite solid-state electrolyte with super flexibility and performance for lithium metal battery. Nano Energy 71. doi:10.1016/j.nanoen.2020.104600
64. Tang W, Tang S, Zhang C, Ma Q, Xiang Q, Yang Y-W, Luo J(2018) Simultaneously Enhancing the Thermal Stability, Mechanical Modulus, and Electrochemical Performance of Solid Polymer Electrolytes by Incorporating 2D Sheets. *8*(24),1800866. doi:https://doi.org/10.1002/aenm.201800866
65. Vahini M, Muthuvinayagam M(2018) AC impedance studies on proton conducting biopolymer electrolytes based on pectin. *Materials Letters, 218*, 197–200. doi:https://doi.org/10.1016/j.matlet.2018.02.011
66. Veena G, Lobo B (2018) AC and DC electrical transport properties of potassium permanganate doped PVA-PVP solid polymer electrolyte. Mater Res Express 6(3):035315. doi:10.1088/2053-1591/aaf7ac
67. Vijaya N, Selvasekarapandian S, Sornalatha M, Sujithra KS, Monisha S (2017) Proton-conducting biopolymer electrolytes based on pectin doped with NH4X (X = Cl, Br). Ionics 23(10):2799–2808. doi:10.1007/s11581-016-

1852-5

68. Wandee Y, Uttapap D, Mischnick P (2019) Yield and structural composition of pomelo peel pectins extracted under acidic and alkaline conditions. Food Hydrocolloids 87:237–244. doi:https://doi.org/10.1016/j.foodhyd.2018.08.017
69. Wang X-Y, Xu R, Wang Y-X, Ma L-Y, Nie S-P, Xie M-Y, Yin J-Y (2020) Physicochemical and rheological properties of pomelo albedo pectin and its interaction with konjac glucomannan. Int J Biol Macromol 151:1205–1212. doi:https://doi.org/10.1016/j.ijbiomac.2019.10.167
70. Yang J-S, Mu T-H, Ma M-M (2018) Extraction, structure, and emulsifying properties of pectin from potato pulp. Food Chem 244:197–205. doi:https://doi.org/10.1016/j.foodchem.2017.10.059
71. Yang X, Nisar T, Liang D, Hou Y, Sun L, Guo Y (2018) Low methoxyl pectin gelation under alkaline conditions and its rheological properties: Using NaOH as a pH regulator. Food Hydrocolloids 79:560–571. doi:https://doi.org/10.1016/j.foodhyd.2017.12.006
72. Youcef HB, Orayech B, Amo D, Bonilla JML, Shanmukaraj F, D., & Armand MJS(2020) Functionalized cellulose as quasi single-ion conductors in polymer electrolyte for all-solid–state Li/Na and LiS batteries. *345*,115168
73. Yusof SZ, Woo HJ, Arof AK (2016) Ion dynamics in methylcellulose–LiBOB solid polymer electrolytes. Ionics 22(11):2113–2121. doi:10.1007/s11581-016-1733-y

Figures

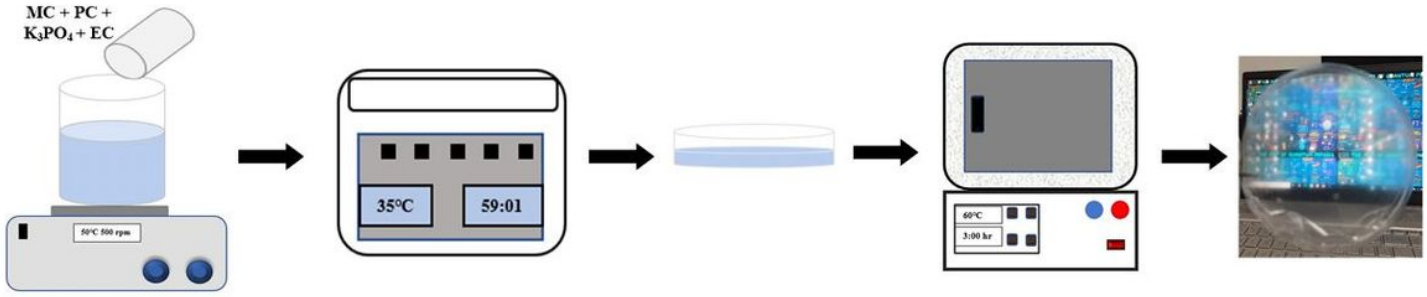

Figure 1

Schematic description of MC/PC/K3PO4/EC CPE preparation

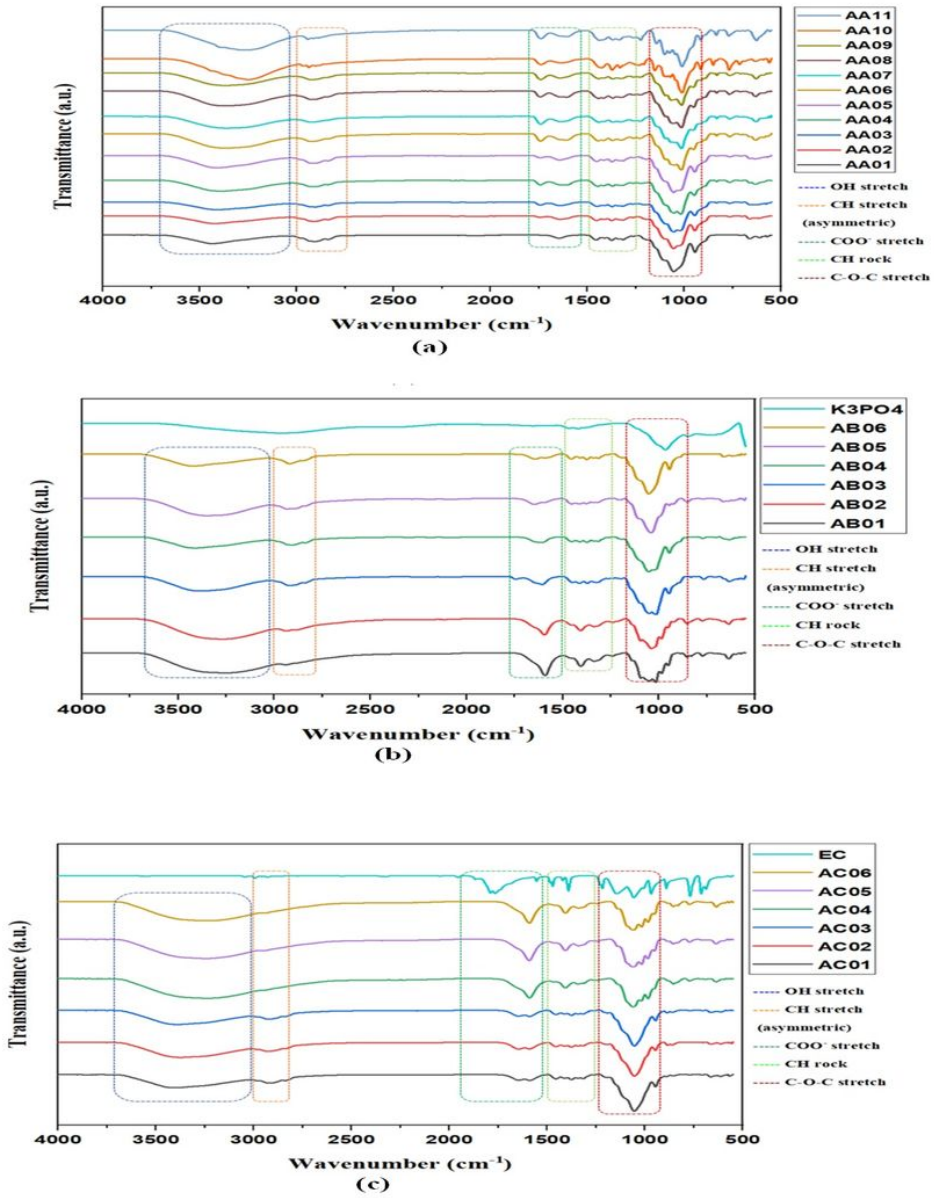

Figure 2

FTIR spectra of MC/PC polymer blend

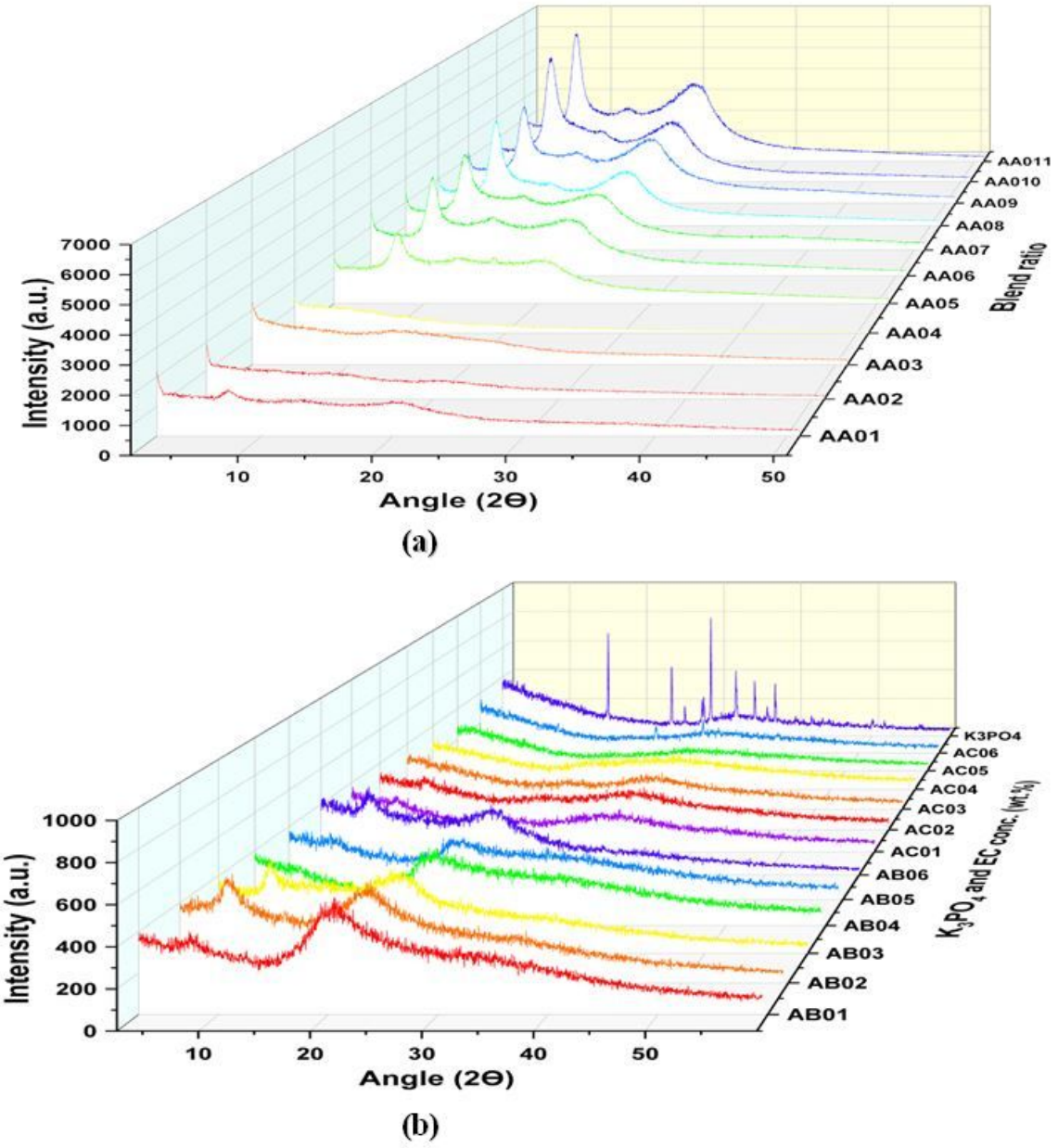

Figure 3

XRD patterns of MC/PC based SBE

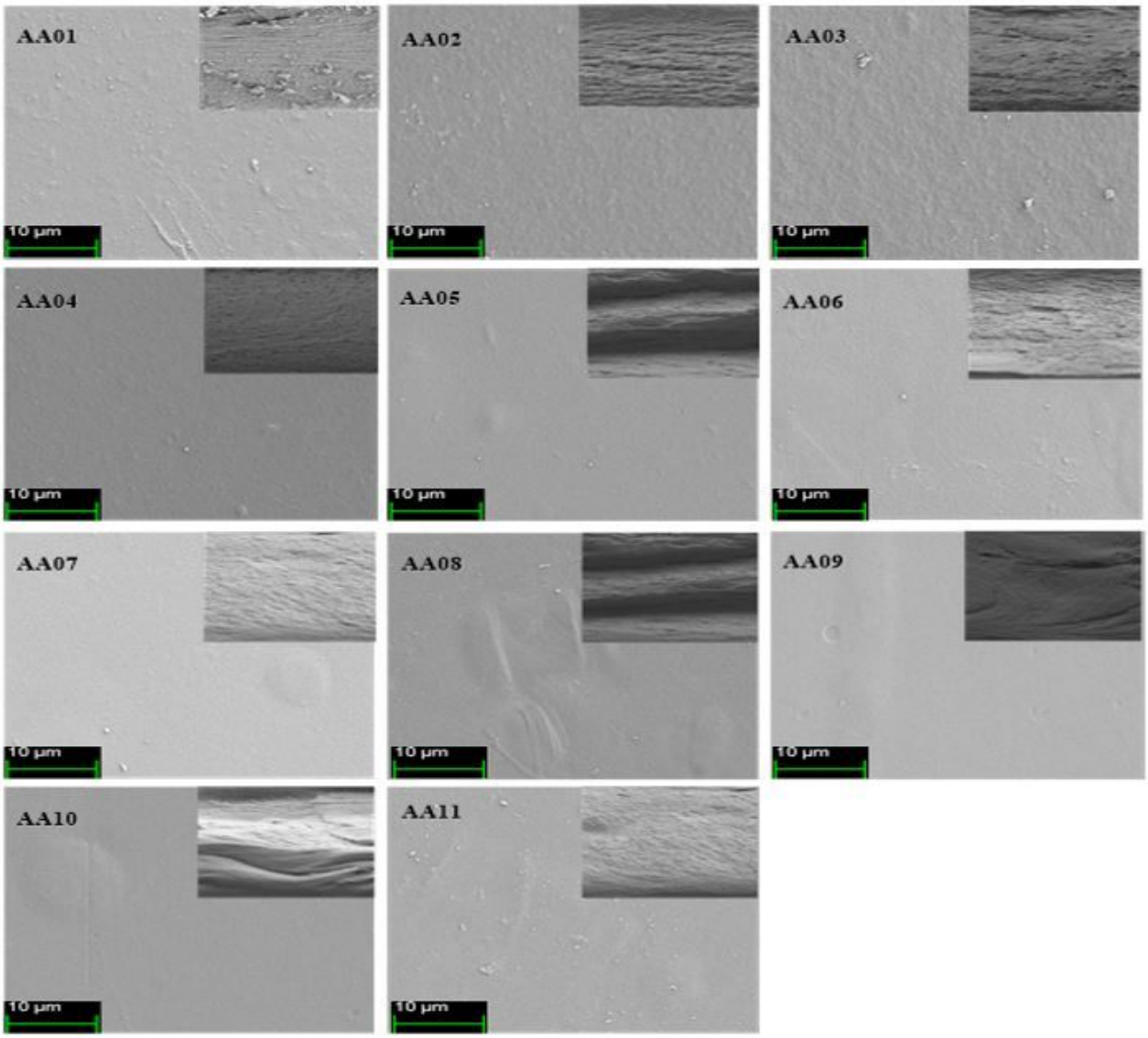

Figure 4

FESEM micrograph showing the surface morphology of MC/PC/K_3PO_4/EC CPEs

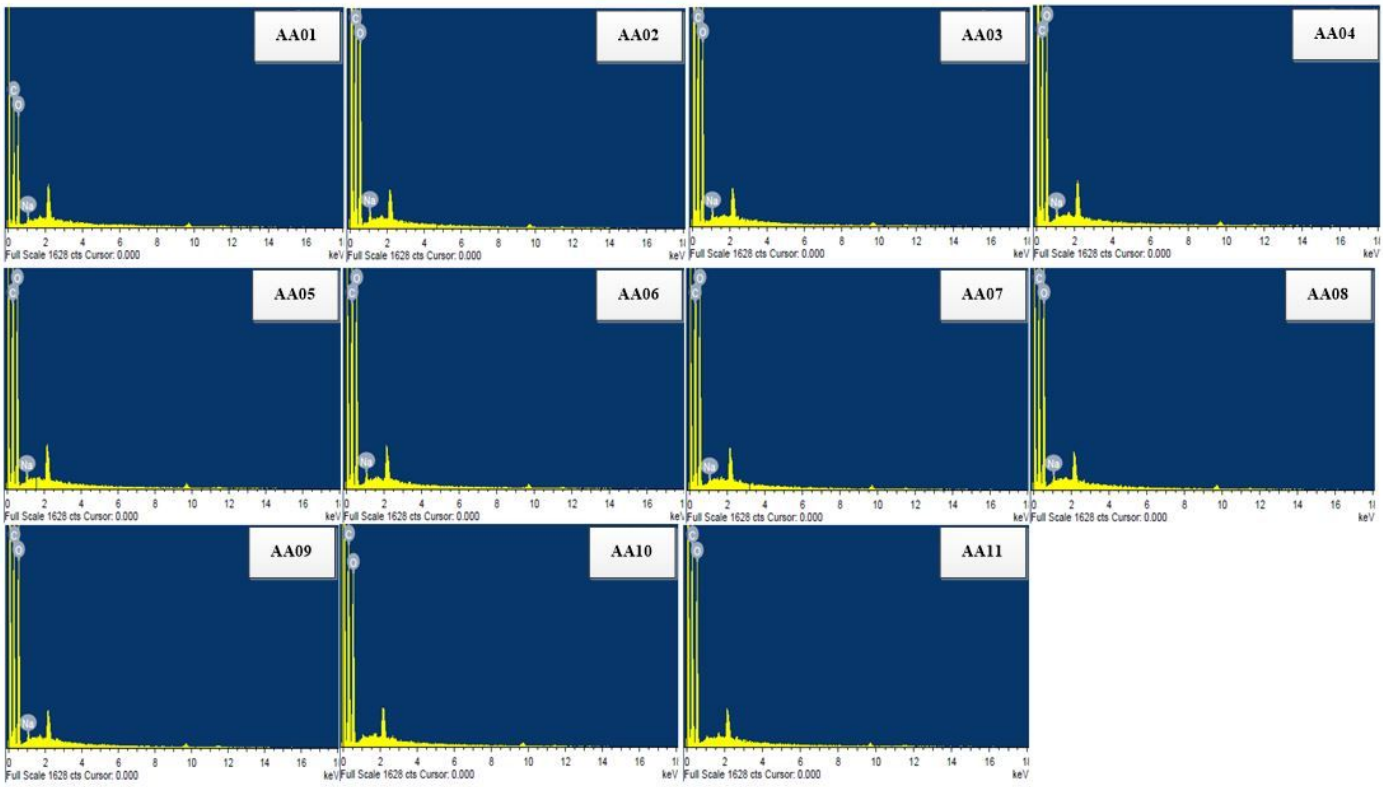

Figure 5

EDX spectra of MC/PC polymer blend

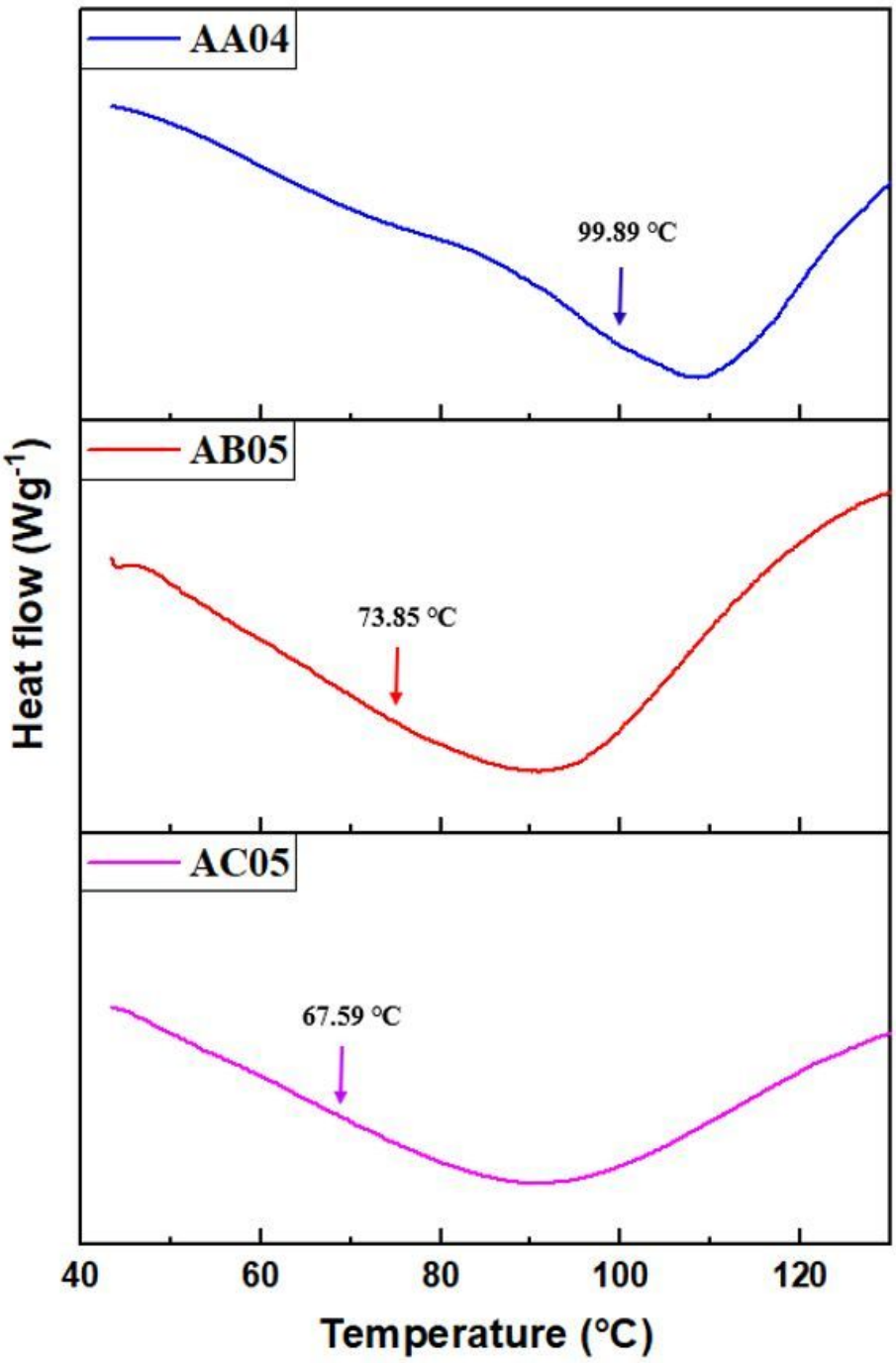

Figure 6

DSC curve indicating the T_g for the prepared CPEs

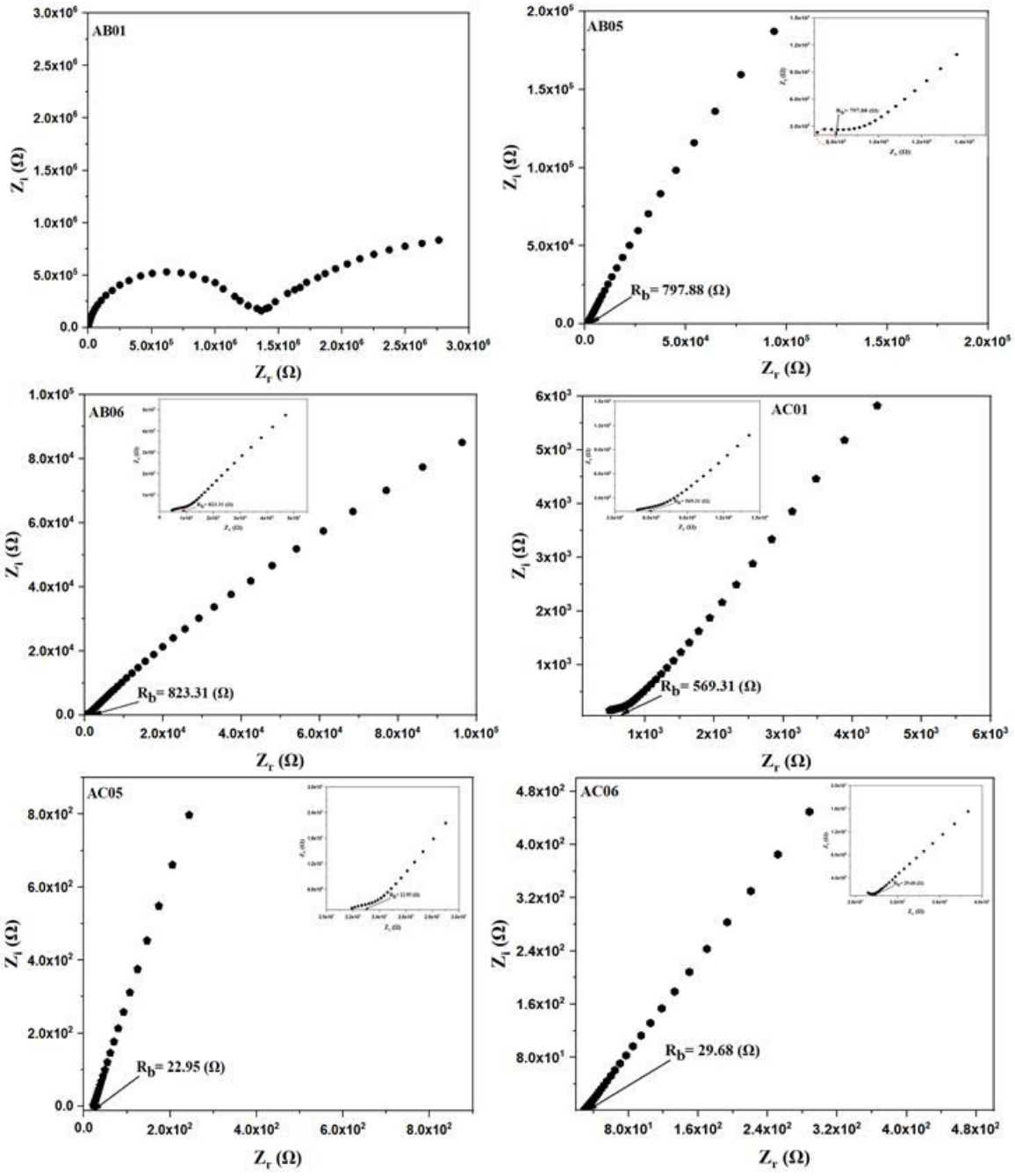

Figure 7

EIS impedance plots of selected MC/PC/K_3PO_4 based CPEs

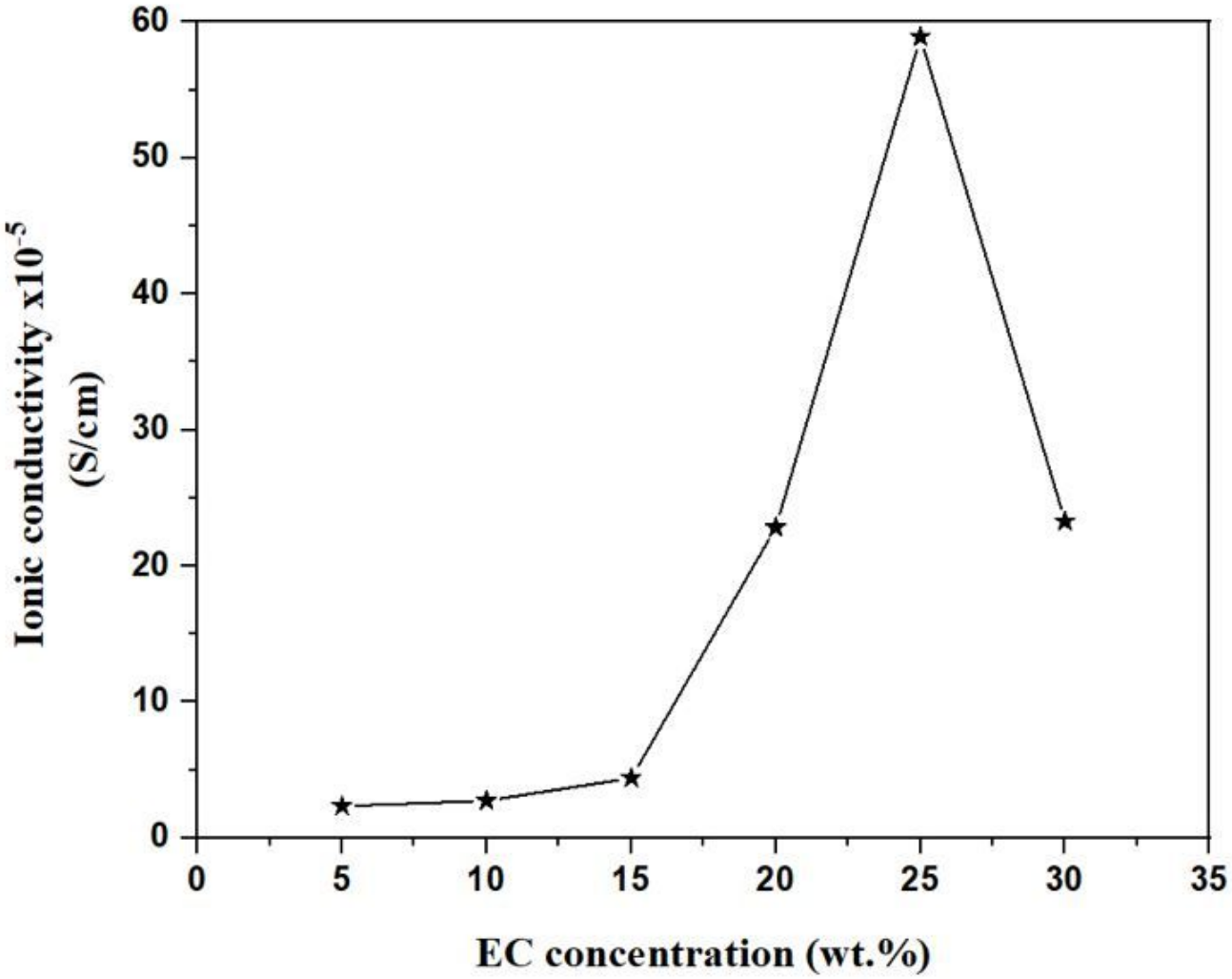

Figure 8

Variation of room temperature conductivity of AC05 as a function of EC concentration

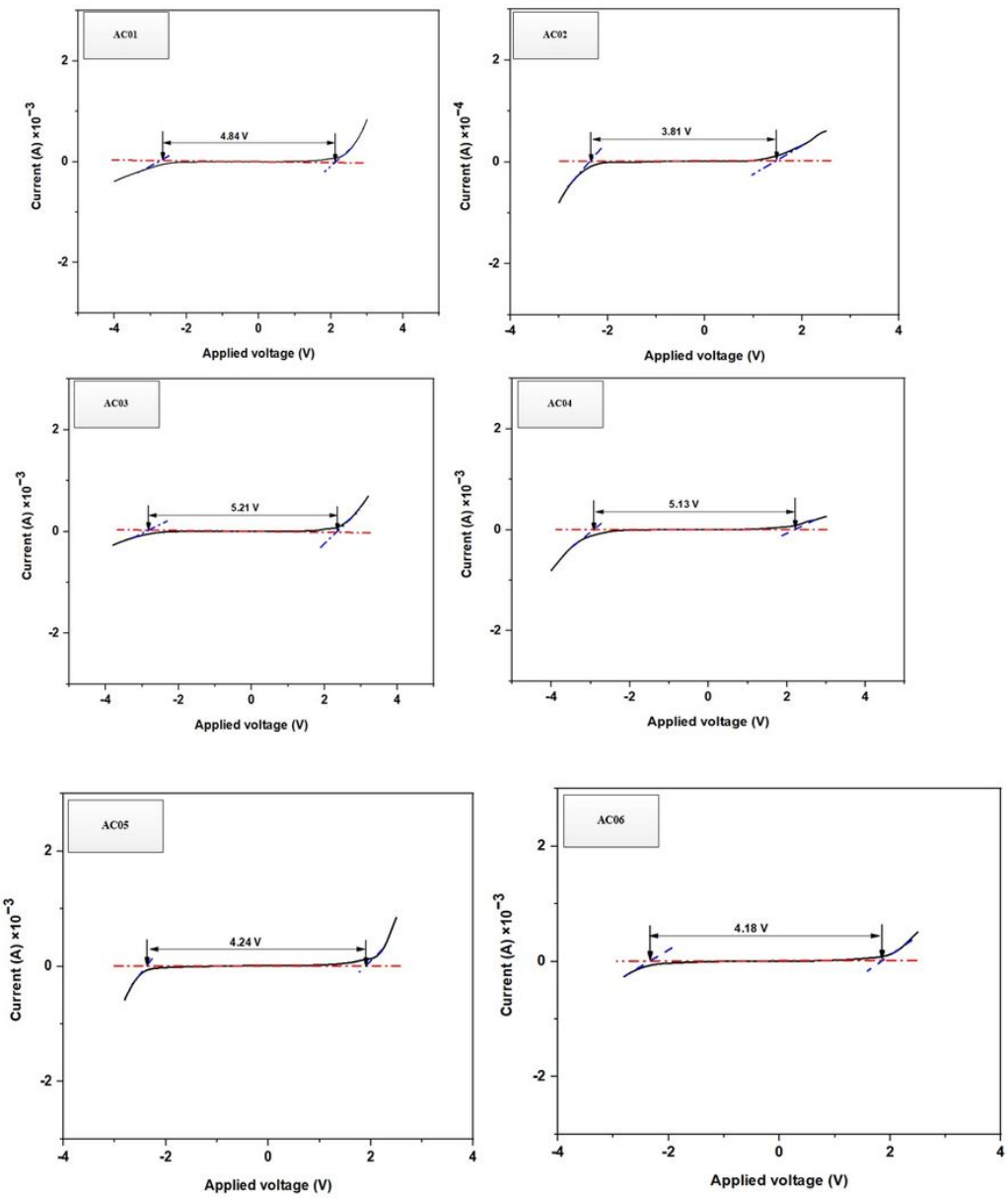

Figure 9

Potential window plots for MC/PC/K_3PO_4/EC CPEs

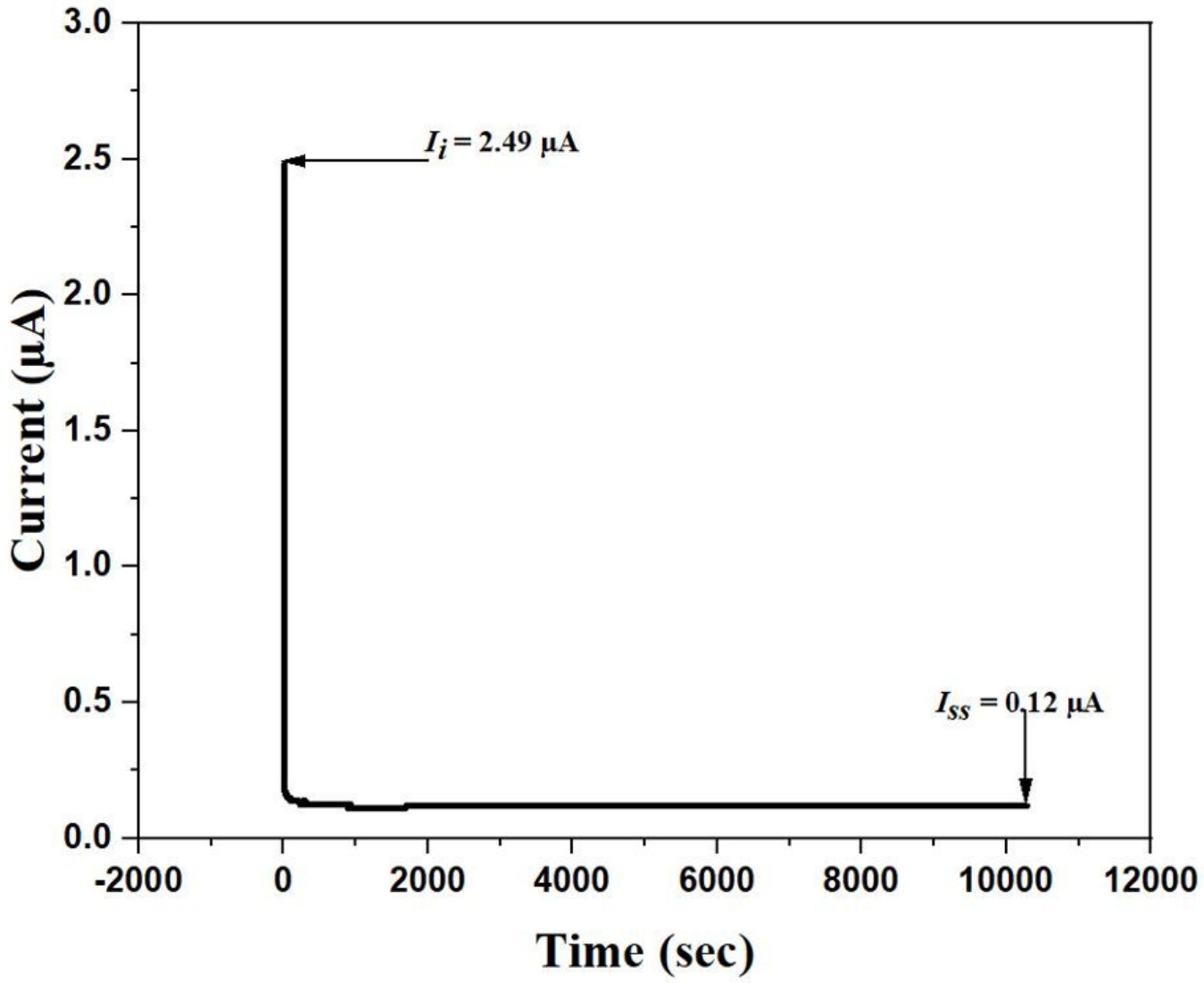

Figure 10

TNM of AC05 showing initial and steady-state currents

Supplementary Files

This is a list of supplementary files associated with this preprint. Click to download.

- MCPCK3PO4ECsupplimentary.docx